Laboratory Realization of an Alfvén Wave Maser

J. E. Maggs and G. J. Morales
Physics and Astronomy Department, University of California, Los Angeles, Los Angeles, California 90095, USA
(Received 3 March 2003; published 18 July 2003)

It is demonstrated that a frequency selective Alfvén-wave resonator can be realized by applying a nonuniform magnetic field to a plasma region bounded between a cathode and a semitransparent mesh anode. When a current threshold is exceeded, selective amplification results in a highly coherent, large amplitude wave that propagates into an adjacent plasma column.

DOI: 10.1103/PhysRevLett.91.035004 PACS numbers: 52.40.Db, 52.25.Os, 52.35.Bj, 52.35.Py

It is well known that the coherent amplification of electromagnetic radiation leading to laser or maser action requires a combination of essential physical processes. These include an active medium where a nonequilibrium population is maintained. Its role is to selectively amplify the wave over a narrow frequency interval. Another element is a partial reflector which plays a dual role. It allows the amplified signal to undergo multiple passes through the active medium, while simultaneously allowing the beam to exit into the region of interest. In working with optical or microwave frequencies the requirements are satisfied with atomic species that exhibit inverted populations within a cavity bounded by suitable mirrors. The present study reports on a laboratory realization of an analogous situation for Alfvén waves. These waves propagate in large magnetized plasmas and play a major role in the dynamics of the auroral ionosphere, the magnetospheres of planets, the surface of stars and the interstellar medium.

Theoretical studies [1–3] have investigated Alfvén wave masers formed in the plasma surrounding the Earth. Similar considerations apply to other magnetized systems in the Universe. Some theories consider the maser cavity formed by the magnetospheric plasma bounded by the reflecting conjugate ionospheres. The nonequilibrium, active material considered is a population of energetic ions [1] in the radiation belt. Another class of Alfvén maser activity occurs at lower altitudes. Because of the spatial variation of the ionospheric plasma parameters, an Alfvén resonator is naturally formed [4–7] between the lower E region of the ionosphere and a region in the topside ionosphere. This higher region acts as a partial reflector that allows amplified signals to propagate into the magnetosphere. Satellite and rocket observations [8,9] in this region are consistent with resonant amplification of Alfvén waves and corroborate ground-based measurements [10,11]. Various nonequilibrium sources have been considered to excite the ionospheric Alfvén resonator. These include the natural magnetospheric convection [4], electron beams [12], lightning discharges [13,14], and powerful high frequency radio signals [15]. In the present laboratory study an equivalent Alfvén resonator is realized in which the nonequilibrium source is a field-aligned current.

The experimental results are obtained in the upgraded Large Plasma Device (LAPD-U) at UCLA [16]. A magnetized plasma column is generated by primary electrons emitted from a cathode. The effective diameter of the plasma column is 30 cm and is determined by the size of the emissive coating applied to the cathode. The primary electrons are accelerated by a potential difference of 45 V applied, on a pulsed basis, between the cathode and a semitransparent copper mesh anode (transmission efficiency $\sim$50%) located 55 cm away. The region between the cathode and anode plays the role of the Alfvén resonator.

The injected currents flowing within the resonator and the region adjacent to the mesh anode range from 6 to 10 kA. The accelerated primaries drift into a vacuum chamber, whose overall axial extent is 19.35 m, and strike neutral He gas at a fill pressure of $1–2 \times 10^{-4}$ Torr to generate a He plasma with a greater than 50% degree of ionization. This is the main plasma region, outside the resonator, in which the measurements of the spontaneously amplified Alfvén waves are made. In this region the plasma density is in the range of $2–3 \times 10^{12}$ cm^{-3}, while the electron temperature is approximately 8 eV with the ion temperature in the range of 1 eV. The current-carrying plasma between the cathode and anode displays slightly different parameter values, which at this stage cannot be measured. It should be emphasized that Alfvén waves can propagate between the cathode-anode region and the main plasma column, with the anode mesh acting as a partially transmitting boundary. This component plays a role analogous to the partially reflecting mirrors used in laser/maser cavities and corresponds to the topside opening of the ionospheric Alfvén resonator.

The plasma column is confined by an axial magnetic field, B_0, generated by an 18 m-long solenoid formed from a total of 90 water-cooled coils. The coils are grouped in carts which are individually fed by regulated power supplies. The variability of the spontaneous amplification of shear Alfvén waves is explored over the range of 500 to 2000 G. These values correspond to the uniform field in

the main plasma column located within the solenoid. Regardless of the uniform-field strength chosen for the main plasma column, the magnetic field strength in the cathode-anode region decreases steadily from the anode toward the cathode surface due to end flaring in the last magnet cart. The field at the cathode is a factor of 0.7 smaller than that at the anode, a value determined by the distance between the cathode and anode. The flaring field plays a crucial role. It acts as an effective low-pass filter that limits the bandwidth of the shear Alfvén waves propagating within the resonator.

The spontaneously amplified magnetic fields are measured with a small magnetic probe (i.e., B-dot loops) inserted into the plasma through a port located at an axial position, z, from the cathode in the equatorial plane of the machine. The probe consists of mutually perpendicular loops ($\sim$4 mm in size) capable of measuring the simultaneous evolution of the three components of the magnetic field fluctuations. The frequency range of the fluctuations investigated here is well separated from the characteristic resonant frequency of each loop.

The broken curve in Fig. 1 displays the spectral amplitude of the transverse component of the magnetic noise observed at $z = 4.9$ m and a radial position corresponding to the center of the plasma for a magnetic field of 1000 G. At this field setting the amplification mechanism is not effective and the behavior sampled is the intrinsic frequency response of the resonator. The frequency axis in Fig. 1 is scaled to the ion cyclotron frequency in the uniform field appropriate to the main column. The two principal features seen are a spectral peak centered around $0.6f_{\rm ci}$, and a strong quenching of the noise for frequencies above $0.7f_{\rm ci}$. The suppression of the noise is quite reminiscent of the effect that would be obtained if a low-pass filter were to be inserted externally in the circuit. In this case the filtering is being accomplished naturally by the flaring magnetic field in the cathode-anode region. The value of $0.7f_{\rm ci}$ corresponds to the highest frequency of a shear Alfvén wave that can propagate within the cathode-anode resonator. This arises because, to lowest order in the transverse wave number $k_\perp$, the axial wave number of a shear Alfvén wave of frequency ω is given by $k_\parallel = \omega/v_A$, where $v_A = c(\Omega_i^2 - \omega^2)^{1/2}/\omega_{\rm pi}$ is the Alfvén speed, with Ω_i the (angular) ion cyclotron frequency and $\omega_{\rm pi}$ the ion plasma frequency. Hence this electromagnetic mode does not propagate for frequencies above the smallest ion cyclotron frequency within the resonator. The spectral peak near $0.6f_{\rm ci}$ corresponds to the lowest resonant mode between the cathode and the mesh anode. The parallel wavelength in the main plasma column is 2.7 m, but is significantly smaller in the region between the anode and the cathode. The spectral enhancement is due to constructive interference after multiple bounces between these boundaries. Also, we have found that the gap between the highest shear wave frequency and the ion cyclotron frequency (i.e., the region between $0.7f_{\rm ci}$ and $f_{\rm ci}$ in Fig. 1) tracks the magnetic field in the region between the anode and cathode and not the field in the main plasma column which indicates that the spectrum observed in the main plasma column is generated in the anode-cathode region.

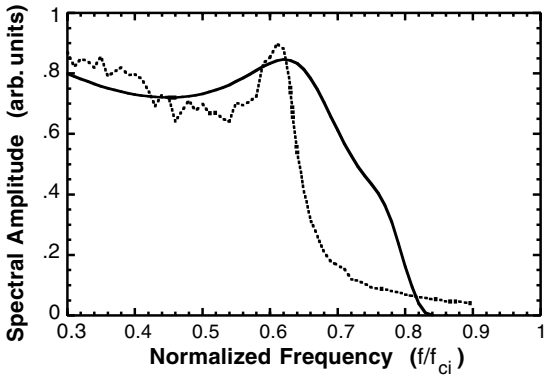

FIG. 1. The broken curve is the ambient noise frequency spectrum at the plasma center at $z = 4.9$ m, $B_0 = 1000$ G. The peak near $0.6f_{\rm ci}$ corresponds to the first resonant Alfvén mode within the cathode-anode cavity. The quenching at higher frequencies results from the nonuniform magnetic field in the cavity. The solid curve is the prediction of a model consisting of partial wave reflections between cathode and anode.

The result of a simple mathematical model for the frequency behavior of the Alfvén resonator is shown as the solid curve in Fig. 1. The quantity plotted is $|\psi|$ where

$$\psi(z,\omega) = \exp\{i[k_r(\omega)L + k_p(\omega)z]\}/\{1 - R_A \exp[i2k_r(\omega)L]\}$$

represents a component of the fluctuating field at frequency ω measured in the main plasma at a distance z. L is the distance between the cathode and anode, and R_A is the reflection coefficient of the anode. The wave numbers in the main plasma and in the resonator are k_p and k_r, respectively. These are calculated locally from the dispersion relation $k_\parallel{}^2\varepsilon_\parallel + k_\perp{}^2\varepsilon_\perp = k_0{}^2\varepsilon_\parallel\varepsilon_\perp$ in which electron-ion Coulomb collisions and ion-neutral collisions are included in the evaluation of the dielectric coefficients $\varepsilon_\parallel$ and $\varepsilon_\perp$. The transverse wave number is $k_\perp = \pi/a$, where a is the plasma radius and $k_0 = \omega/c$. It is seen that the key features of the measured noise spectrum are reproduced. The peak near $0.6f_{\rm ci}$ is the resonant mode and the quenching at higher frequencies is a direct consequence of the evanescence predicted by the dispersion relation. The agreement between the model and the shape of the observed noise spectrum supports the notion that an effective Alfvén resonator is achieved in this cathode-anode configuration.

The spontaneous amplification of the resonant mode is observed to occur for selective values of the confinement magnetic field and the plasma current. Spectacular flares of extremely coherent signals develop at low magnetic fields and relatively large plasma currents, i.e., as the ratio of the electron drift-velocity to the phase velocity of the

first resonant mode is increased. The middle panel in Fig. 2 displays the temporal behavior of one transverse component of the fluctuating magnetic field measured at the plasma center at $z = 8.75$ m for $B_0 = 700$ G. The bottom panel shows the discharge current over the same time scale. It is seen that the magnetic signal exhibits an explosive growth as the discharge current reaches a level of approximately 7000 A. The growth saturates within 0.5 msec, and after that the mode exhibits a slow decay. Eventually the amplitude of the mode returns to the ambient noise level and results in the spectral features characterized in Fig. 1. The maser flare occurs dependably if the current threshold is exceeded.

The top panel in Fig. 2 provides an expanded view of the temporal behavior of the flare over an interval of 0.1 msec. It shows that the flaring mode is monochromatic and remarkably coherent. The frequency of the flaring signal corresponds to $0.6 f_{ci}$ and is the same as the frequency of the resonant mode. The envelope of the actual flare signal is smooth, and not jagged, as appears in the middle panel of Fig. 2 due to under sampling of the original time trace in producing the figure.

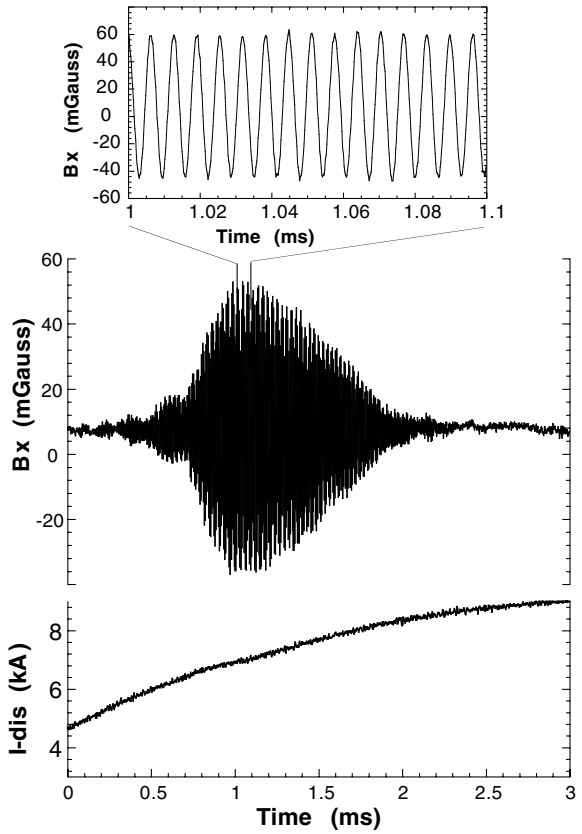

FIG. 2. Middle panel: single-shot temporal evolution of the horizontal component of the magnetic field. Center of the plasma, $z = 8.75$ m, $B_0 = 700$ G. Bottom panel: time dependence of current injected by cathode into plasma column. Top panel: expanded temporal behavior showing remarkable coherency. Frequency corresponds to that of the mode with a spectral peak around $0.6 f_{ci}$ in Fig. 1.

The spatial profile of the spontaneously amplified mode along a horizontal cut across the confinement field is shown in Fig. 3. This figure displays the measured spectral amplitude of the perpendicular component of the fluctuating magnetic field at a time corresponding to the peak of the flare. It is found that the flare is a global mode and that its spatial pattern is similar to that exhibited by the spectral peak at $0.6 f_{ci}$, as documented for ambient noise conditions. The polarization properties of the flare are shown by the hodograms in Fig. 3 for three locations across the plasma column. The direction of the confinement field is such that in this figure counter clockwise rotation corresponds to a mode with left-handed polarization.

The detailed time evolution of the flare at horizontal location $x = 39$ cm is documented in Fig. 4. It displays the time evolution of the x component of the flaring field during two intervals, one starting before the peak is reached (solid curve) and the other starting after the peak is reached (dotted curve). The time axis starts at -0.2 m sec and at $+0.7$ m sec, accordingly. The two traces have been aligned at their start to test for frequency variations. It is seen that while the flaring mode is extremely coherent, as the system evolves there is a small decrease in the frequency of the mode that is demonstrated by the two signals getting out of phase. It is likely that the frequency drift results from slowly changing plasma parameters. Also, it is likely the flaring phenomena result from being near threshold where changes in plasma parameters as the current increases are enough to quench the maser.

With the insight gained on the role of the cathode-anode region in creating a resonant cavity for shear Alfvén waves, it is appropriate to think of the flare phenomenon as an instability that drives cavity modes

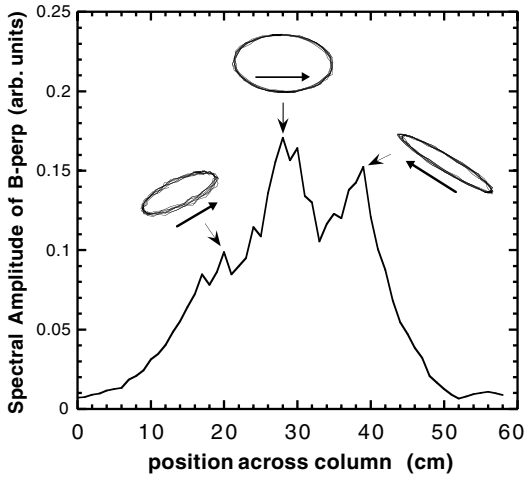

FIG. 3. Spatial properties of flaring mode. The lower curve is the dependence of spectral amplitude on the horizontal position across the plasma column (the plasma center is at 32 cm). The hodograms show transverse polarization at the various horizontal positions.

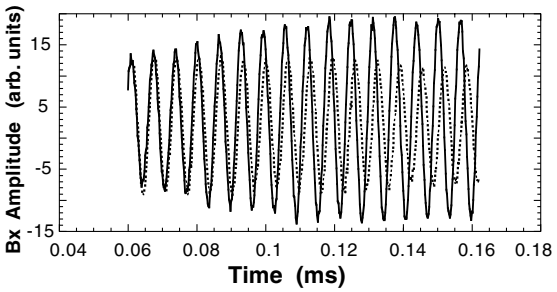

FIG. 4. A slow temporal decrease in the frequency of flaring mode is shown. The time traces of the Bx component are compared starting 0.2 ms before the peak of the flare (solid curve), and starting 0.7 ms after the peak (dotted curve).

when a threshold condition is exceeded. A candidate for the underlying instability is the background electron drift induced on the plasma column. This arises in order to achieve the net zero-current condition associated with the floating boundary located 18 m away from the anode. This possible scenario is illustrated in Fig. 5 where the solid curve corresponds to the resonant-phase condition, i.e., $k_r(\omega)L/\pi - 1$. Perfect resonance corresponds to the value of this quantity being equal to zero.

The family of broken curves in Fig. 5 corresponds to the quantity $-\partial f_0/\partial v$ evaluated at the phase velocity ω/k_r. This quantity is shown in an arbitrary value scale to make the comparison more evident since what is relevant is the transition from positive to negative values. A positive value for this quantity implies the mode is damped while a negative value represents growth. The zero crossing determines the threshold condition for instability. The electron distribution function f_0 is taken as a shifted Maxwellian with a drift velocity v_D determined

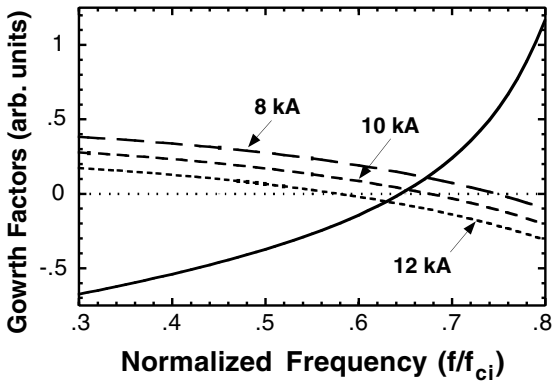

FIG. 5. Flare model in which instability due to electron drift drives a shear Alfvén wave that experiences partial reflection. The solid curve is the resonant phase difference of the mode. Broken curves are proportional to the negative of the slope of the electron distribution function evaluated at the phase velocity for a given frequency. The numbers correspond to the current injected at the cathode.

by the current I injected by the cathode, namely $v_D = I/(en_0\pi a^2)$, where n_0 is the plasma density and e the quantum of charge.

It is seen from Fig. 5 that as the current is increased over the range of 8–12 kA the damped waves become unstable. The unstable region overlaps with the resonant mode condition in the frequency interval close to $0.6f_{ci}$. This parametric dependence follows the general trend of the data in Fig. 2. Of course, a closer quantitative match requires a more detailed theory that includes gradient effects.

In summary, it has been shown that an Alfvén resonator can be realized in the laboratory and that when it is subjected to nonequilibrium conditions, it develops coherent amplification analogous to the behavior proposed for natural Alfvén wave masers.

This work is sponsored by NSF and ONR. The experiment was performed in the Basic Plasma Science Facility (BAPSF) operated at UCLA under joint sponsorship of NSF and DOE. The authors thank Dr. D. Leneman for comments concerning the role of the cathode-anode region and Mr. M. VanZeeland for providing a magnetic probe of small dimension.

[1] S. V. Polyakov, V. O. Rapoport, and V. Yu. Trakhtengerts, Fiz. Plazmy **9**, 371 (1983).
[2] P. P. Belyaev, S. V. Polyakov, V. O. Rapoport, and V. Yu. Trakhtengerts, Geomagn. Aeron. **24**, No. 2 (1984).
[3] P. P. Belyaev, S. V. Polyakov, V. O. Rapoport, and V. Yu. Trakhtengerts, Izv. Vyssh. Uchebn. Zaved. Radiofiz. **33**, 408 (1990).
[4] V. Yu. Trakhtengerts and A. Ya. Feldstein, J. Geophys. Res. **96**, 19363 (1991).
[5] B. J. Thompson and R. L. Lysak, J. Geophys. Res. **101**, 5359 (1996).
[6] R. L. Lysak, J. Geophys. Res. **104**, 10017 (1999).
[7] O. A. Pokhotelov, D. Pokhotelov, A. Streltsov, V. Khruschev, and M. Parrot, J. Geophys. Res. **105**, 7737 (2000).
[8] M. Grzesiak, Geophys. Res. Lett. **27**, 923 (2000).
[9] N. Ivchenko, G. Marklund, K. Lynch, D. Pietrowski, R. Torbert, F. Primdahl, and A. Ranta, Geophys. Res. Lett. **26**, 3365 (1999).
[10] P. P. Belyaev, T. Bosinger, S. V. Isaev, and J. Kangas, J. Geophys. Res. **104**, 4305 (1999).
[11] F. Z. Feygin, A. K. Nekrasov, K. Mursula, J. Kangas, and T. Pikkarainen, T. Ann. Geophys. **12**, 147 (1994).
[12] N. G. Lekhtinen, G. A. Markov, and S. M. Fainstein, Izv. Vyssh. Uchebn. Zaved. Radiofiz. **38**, 312 (1995).
[13] H. Fukunishi, Y. Takahashi, M. Sato, A. Shone, M. Fujito, and Y. Watanabe, Geophys. Res. Lett. **24**, 2973 (1997).
[14] A. I. Sukhorukov and P. Stubbe, Geophys. Res. Lett. **24**, 829 (1997).
[15] V. Yu Trakhtengerts, Geomagn. Aeron. **29**, No. 3 (1989).
[16] http://plasma.physics.ucla.edu/BAPSF